J Eng Math: (2022) 134:6

https://doi.org/10.1007/s10665-022-10226-7



Influence of asymptotically-limiting micromechanical properties on the effective behaviour of fibre-supported composite materials

Eleanor A. Doman · Rebecca J. Shipley · Nicholas C. Ovenden

Received: 25 January 2022 / Accepted: 10 May 2022

© The Author(s) 2022

Abstract The macroscale tensile behaviour of slender fibre-supported composite bodies is examined via an asymptotic homogenisation approach. A series of semi-analytic three-dimensional models for linearly elastic fibre-reinforced materials under extreme, but realistic, limiting microscale mechanical properties are derived, and implemented using COMSOL Multiphysics. The key limits investigated are cases involving incompressibility of one component material, and those where dramatic differences in the shear moduli of the component materials exist within the composite body. Discrepancies are observed between the effective macroscale properties obtained from a standard model, based on the published literature, and those obtained from the models of micromechanical limiting behaviours derived here. Such discrepancies have significant implications when using such models to optimise the material properties of composite materials.

Keywords Asymptotic homogenisation · Heterogeneous composites · Multiscale modelling

1 Introduction

A composite material has a structure composed of two or more distinct base materials with different chemical and/or physical properties. Such composite materials have a wide variety of different applications across all areas of engineering. Examples of man-made composite materials include reinforced concrete used in infrastructure, carbon- or glass-reinforced polymers used in transport and energy projects [1,2], and new hydrogel-based materials for use in tissue engineering applications [3]. Across all such examples, the microscale mechanical properties are integral to their function [2,4,5]. By combining multiple materials and structures, the mechanical properties of the overall composite material are able to be specialised and refined beyond what is possible with a single material component alone [3,6,7].

E. A. Doman (⋈)· N. C. Ovenden

Department of Mathematics, University College London, Gower St, London WC1E 6BT, UK e-mail: eleanor.doman@manchester.ac.uk

N. C. Ovenden

e-mail: n.ovenden@ucl.ac.uk

Published online: 27 May 2022

R. J. Shipley

Department of Mechanical Engineering, University College London, Torrington Place, London WC1E 7JE, UK

6 Page 2 of 24 E. A. Doman et al.

Mathematical modelling can reduce the time and cost of optimising the mechanical properties of a composite material for their respective applications. Many composite materials are constructed using materials and structures across disparate length scales. These materials often seek to emulate hierarchical materials from nature, despite the fact that the mechanical properties of the component parts are very hard to fully quantify due to the difficulty of measuring mechanical properties at micrometre or smaller scales using standard experimental techniques [8,9]. It is therefore important to develop mathematical modelling frameworks that can describe complex multiscale composite materials in a computationally efficient fashion, while not imposing restrictive geometric assumptions that, in turn, inhibit the generalisability of such modelling techniques.

The problem of simulating and optimising the mechanical properties of multiscale composite structures of materials has been addressed in numerous studies over recent years [10–15]. A wide range of methods have been used including imaging informed direct numerical simulation down to very fine scales [16–18], area-weighted averaging methods [19,20], complex micromechanical regimes [21-24] and asymptotic homogenisation [25-29]. Each of these methods comes with strengths and weaknesses in terms of physical accuracy, amount of information required and computational complexity. Of particular interest in this paper is the method of asymptotic homogenisation, due to its focus on multiple scales within composite materials. Asymptotic homogenisation is an upscaling method that uses asymptotic methods to derive equations describing macroscale behaviour while still factoring in geometric and physical effects on the microscale, as well as the inherent scaling behaviours of the system [30]. This may yield more sophisticated macroscale constitutive relationships, for example relating stress and strain, than would be assumed using simpler approaches; a classic example of this is the derivation of poroelastic macroscale equations in the work of Burridge and Keller, [31]. Asymptotic homogenisation has more recently been used to develop semianalytic mechanical models for composite materials [27,32,33]. One of the core assumptions of these asymptotic homogenisation techniques is the requirement of a periodic microscale. Periodicity reduces the computational cost significantly by removing the requirement to use a fine scale mesh across the whole domain, but this naturally restricts the applicability of the method.

In this paper, we theoretically examine the macroscale tensile behaviour of slender fibre-supported composite bodies using an asymptotic homogenisation approach. By developing a semi-analytic three-dimensional model for a linearly, elastic, fibre-reinforced material, we demonstrate that certain limiting cases of the material properties in the microscale lead to discrepancies in the derived effective macroscale properties. This occurs particularly in situations where the component materials have extreme differences in terms of their compressibility or shear moduli. Such observed discrepancies have important implications to those using asymptotic homogenisation models for optimising composite material properties. Reasons for why such discrepancies arise are explained and guidance is offered on the microscale parameter regimes where an alternative modelling approach to determining macroscopic properties should perhaps be considered.

In Sect. 2, asymptotic homogenisation is used to develop a semi-analytic 3D model for a slender, linearly, elastic, composite, fibre-reinforced material, building on an established literature around homogenisation methods for linearly elastic composite solids [25–29,34]. The Standard Asymptotic Homogenised Model (SAH model) using the Navier equation is derived assuming dominant scalings of unknown non-dimensional constants and this model is shown to be equivalent to homogenised approaches developed in [26] and [27]. In Sects. 3 and 4, alternative scalings of the non-dimensional constants are considered, particularly (i) the interaction between a compressible and an incompressible material in the microstructure and (ii) the case of a very large difference in shear moduli between the two component materials. In Sect. 5, numerical results are presented showing the effective Young's modulus and Poisson ratio determined by the models in Sects. 3 and 4, and these results are compared with those determined from the Standard Asymptotic Homogenised Model in Sect. 2. Explanations are offered for the numerically observed differences in macroscale behaviour and further discussion and conclusions are provided in Sect. 6.



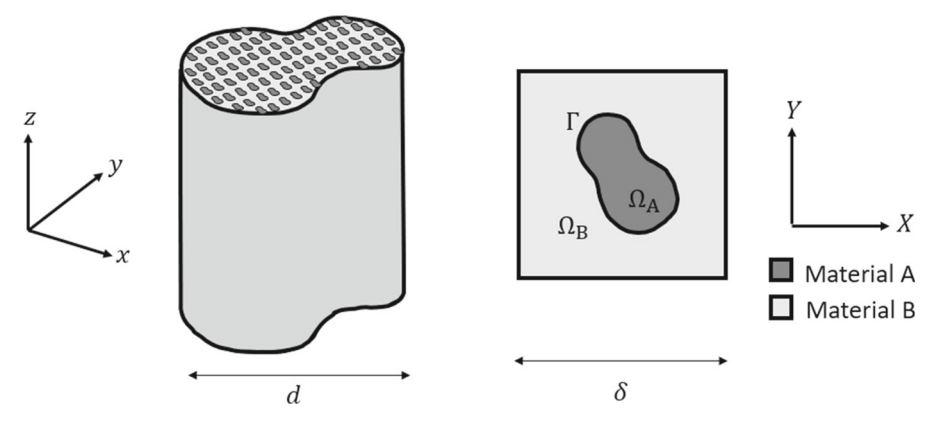


Fig. 1 Schematic representations of example macroscale (left) and microscale (right) geometries. The macroscale is a composite body comprised of two materials, **A** and **B**, represented in dark and light grey, respectively (left). The microstructure is assumed periodic, comprised of a spatially-repeating combination of materials **A** and **B**

2 Standard asymptotic homogenised model

In order to examine the effects of incorporating extreme micromechanical limits into a macroscale model via asymptotic homogenisation, individually tailored models are developed for each specific case. In this section we begin by deriving the SAH model, where the micromechanical scaling parameters are assumed to be of an equivalent order to the dimensional scalings used in asymptotic homogenisation. The SAH is consistent with the established literature [26,27], but a specific notation and method are adopted throughout this paper to enable a direct comparison with the specialised cases explored in Sects. 3 and 4.

Consider a composite cylindrical slender body of arbitrary cross-section made up of two linearly elastic compressible materials A and B, as depicted in the schematic in Fig. 1. The composite material is comprised of fibres of material A embedded in material B, and running parallel to the axis of the cylinder (denoted z in Fig. 1). We assume that the cross-section geometry (in the x-y plane) can be treated as uniform across the length of the cylinder. We also assume that the diameter of these fibres is small compared to the cylinder cross-section, so that the microstructure can be described as a spatially periodic 2D plane constructed from the repeating cells, as shown in the right-hand schematic in Fig. 1.

We denote the microscale coordinates by $\mathbf{X} = (X, Y)^{\mathrm{T}}$ and the longitudinal displacement by z. The mechanical behaviour of material A at the microscale in region Ω_A is described by the dimensional Navier equations,

$$(\lambda_A + \mu_A) \left(\frac{\partial^2 u_i^{A*}}{\partial X_k^* \partial X_i^*} + \frac{\partial^2 w^{A*}}{\partial X_k^* \partial z^*} \right) + \mu_A \left(\frac{\partial^2 u_k^{A*}}{\partial X_i^* \partial X_i^*} + \frac{\partial^2 u_k^{A*}}{\partial z^{*2}} \right) = 0, \tag{1}$$

and

$$(\lambda_A + \mu_A) \left(\frac{\partial^2 u_i^{A*}}{\partial z^* \partial X_i^*} + \frac{\partial^2 w^{A*}}{\partial z^{*2}} \right) + \mu_A \left(\frac{\partial^2 w^{A*}}{\partial X_i^* \partial X_i^*} + \frac{\partial^2 w^{A*}}{\partial z^{*2}} \right) = 0, \tag{2}$$

where k, i = 1, 2 and * denotes a dimensional variable. Here, $\mathbf{u}^A = (u^A, v^A)^T$ is the transverse displacement and w^A is the longitudinal displacement. The Lamé parameters for material A are λ_A and μ_A . An analogous set of Navier equations is used to describe material B in region Ω_B , using counterpart notation. The natural boundary conditions on the microscale interface between A and B, Γ , are continuity of displacement $u_k^{A*} = u_k^{B*}$ and $w^{A*} = w^{B*}$, and continuity of normal stress $\tau_{ik}^{A*}n_i = \tau_{ik}^{B*}n_i$, where τ_{ik} for i, k = 1, 2, 3 is the standard 3D linear elastic stress tensor (see below), n_i for i = 1, 2, 3 denotes the normal vector to the interface, and we assume $n_3 = 0$ given our



6 Page 4 of 24 E. A. Doman et al.

geometrical assumptions. The stress tensor for material A is given by

$$\tau_{ij}^{A*} = \lambda \delta_{ij} \left(\frac{\partial u_k^{A*}}{\partial X_k^*} + \frac{\partial w^{A*}}{\partial z^*} \right) + \mu_A \left(\frac{\partial u_i^{A*}}{\partial X_j^*} + \frac{\partial u_j^{A*}}{\partial X_i^*} \right), \tag{3}$$

$$\tau_{i3}^{A*} = \tau_{3i}^{A*} = \mu_A \left(\frac{\partial u_i^{A*}}{\partial z^*} + \frac{\partial w^{A*}}{\partial X_i^*} \right),\tag{4}$$

and

$$\tau_{33}^{A*} = \lambda_A \left(\frac{\partial u_k^{A*}}{\partial X_k^*} + \frac{\partial w^{A*}}{\partial z^*} + 2\mu_A \frac{\partial W^{A*}}{\partial z^*} \right),\tag{5}$$

with similar relations for the stress tensor components for material B.

2.1 Multiscale analysis

We denote the typical microscale width by δ and the length of the cylinder by d, as depicted in Fig. 1. The governing equations (1), (2) are next non-dimensionalised to evaluate the dominant balance of physical effects, using the following rescalings:

$$X_i^* = \delta X_i, \quad z^* = dz, \quad u_k^{A*} = du_i^A, \quad u_k^{B*} = du_i^B, \quad w^{A*} = dw^A, \quad w^{B*} = dw^B.$$
 (6)

Here, $\epsilon = \frac{\delta}{d}$ represents the ratio of the microscale width to its length, so is much smaller than 1, and we define the non-dimensional constants which represent $\alpha_A = \frac{\lambda_A}{\mu_A}$, $\alpha_B = \frac{\lambda_B}{\mu_B}$ and $\mu = \frac{\mu_A}{\mu_B}$. Note that we may use the stress equations (3)–(5) to see that $\tau_{ij}^{\Omega*} = \mu_{\Omega} \epsilon^{-1} \tau_{ij}^{\Omega}$ for $\Omega = A$ or B. The effective macroscale parameters such as Young's Modulus and Poisson ratio are highly dependent on the microscale mechanical properties and are challenging to estimate. We will therefore explore different scalings of these non-dimensional constants to test different potential behaviours of the model system.

We introduce the macroscale variable $x_k = \epsilon X_k$, and assume that the length scales are disparate so that x_k and X_k may be treated as independent variables. Under this assumption, the governing equations in Ω_A become

$$(1 + \alpha_A) \left(\frac{\partial}{\partial X_k} + \epsilon \frac{\partial}{\partial x_k} \right) \left(\frac{\partial u_i^A}{\partial X_i} + \epsilon \frac{\partial u_i^A}{\partial x_i} + \epsilon \frac{\partial w^A}{\partial z} \right)$$

$$+ \frac{\partial^2 u_k^A}{\partial X_i \partial X_i} + 2\epsilon \frac{\partial^2 u_k^A}{\partial X_i \partial x_i} + \epsilon^2 \frac{\partial^2 u_k^A}{\partial x_i \partial x_i} + \epsilon^2 \frac{\partial^2 u_k^A}{\partial z^2} = 0$$

$$(7)$$

and

$$\frac{\partial^2 w^A}{\partial X_i \partial X_i} + 2\epsilon \frac{\partial^2 w^A}{\partial X_i \partial x_i} + \epsilon^2 \frac{\partial^2 w^A}{\partial x_i \partial x_i} + \epsilon (1 + \alpha_A) \left(\frac{\partial^2 u_i^A}{\partial z \partial X_i} + \epsilon \frac{\partial^2 u_i^A}{\partial z \partial x_i} \right) + \epsilon^2 (2 + \alpha_A) \frac{\partial^2 w^A}{\partial z^2} = 0,$$
(8)

with counterpart equations in Ω_B and boundary conditions on Γ such that

$$u_i^A = u_i^B, \quad w^A = w^B, \quad \text{and} \quad \mu \tau_{ij}^A n_i = \tau_{ij}^B n_i,$$
 (9)

where

$$\tau_{ij}^{A} = \delta_{ij}\alpha_{A} \left(\frac{\partial u_{k}^{A}}{\partial X_{k}} + \epsilon \frac{\partial u_{k}^{A}}{\partial x_{k}} + \epsilon \frac{\partial w^{A}}{\partial z} \right) + \frac{\partial u_{i}^{A}}{\partial X_{j}} + \epsilon \frac{\partial u_{i}^{A}}{\partial X_{j}} + \epsilon \frac{\partial u_{j}^{A}}{\partial X_{i}} + \epsilon \frac{\partial u_{j}^{A}}{\partial x_{i}}, \tag{10}$$

$$\tau_{3i}^{A} = \tau_{i3}^{A} = \frac{\partial w^{A}}{\partial X_{i}} + \epsilon \frac{\partial w^{A}}{\partial x_{i}} + \epsilon \frac{\partial u_{i}^{A}}{\partial z},\tag{11}$$

$$\tau_{33}^{A} = \alpha_{A} \left(\frac{\partial u_{k}^{A}}{\partial X_{k}} + \epsilon \frac{\partial u_{k}^{A}}{\partial x_{k}} \right) + \epsilon (2 + \alpha_{A}) \frac{\partial w^{a}}{\partial z}, \tag{12}$$



and counterpart expressions for the stress tensors in material B. We perform asymptotic expansions of all variables in the form

$$f(\mathbf{x}, \mathbf{X}, z) = f^{(0)}(\mathbf{x}, \mathbf{X}, z) + \epsilon f^{(1)}(\mathbf{x}, \mathbf{X}, z) + \epsilon^2 f^{(2)}(\mathbf{x}, \mathbf{X}, z) + \dots,$$
(13)

where we assume that all variables are periodic in X. Next we equate coefficients of different powers of ϵ in turn to evaluate the behaviour of the system.

Equating coefficients of powers of ϵ^0 in (7), (8), the leading-order governing equations are given by

$$\frac{\partial \tau_{ij}^{A(0)}}{\partial X_i} = \frac{\partial \tau_{i3}^{A(0)}}{\partial X_i} = \frac{\partial \tau_{ij}^{B(0)}}{\partial X_i} = \frac{\partial \tau_{i3}^{B(0)}}{\partial X_i} = 0.$$

$$(14)$$

Combining this with the leading-order boundary conditions from (9), evaluated using the Divergence Theorem and assuming that all variables are periodic on the microscale, we see that $u_k^{A(0)} = u_k^{B(0)} = u_k^{(0)}(\mathbf{x},z)$ and $w^{A(0)} = w^{B(0)} = w^{(0)}(\mathbf{x},z)$, so that the leading-order displacements are locally constant.

2.2 Deriving the microscale cell problem

Equating coefficients of powers of ϵ in the governing equations (7), (8) and boundary conditions (9), we obtain

$$(1 + \alpha_A) \frac{\partial^2 u_i^{A(1)}}{\partial X_k \partial X_i} + \frac{\partial^2 u_k^{A(1)}}{\partial X_i \partial X_i} = 0 \quad \text{and} \quad \frac{\partial^2 w^{A(1)}}{\partial X_i \partial X_i} = 0, \tag{15}$$

on Ω_A , subject to boundary conditions on Γ such that

$$u_k^{A(1)} = u_k^{B(1)}, \quad w^{A(1)} = w^{B(1)}, \quad \text{and} \quad \mu \tau_{ij}^{A(1)} n_i = \tau_{ij}^{B(1)} n_i,$$
 (16)

where

$$\tau_{ij}^{A(1)} = \alpha_A \delta_{ij} \left(\frac{\partial u_k^{A(1)}}{\partial X_k} + \frac{\partial u_k^{(0)}}{\partial x_k} + \frac{\partial w^{(0)}}{\partial z} \right) + \frac{\partial u_i^{A(1)}}{\partial X_j} + \frac{\partial u_j^{A(1)}}{\partial X_i} + \frac{\partial u_i^{(0)}}{\partial x_j} + \frac{\partial u_j^{(0)}}{\partial x_i}, \tag{17}$$

and

$$\tau_{i3}^{A(1)} = \frac{\partial w^{A(1)}}{\partial X_i} + \frac{\partial w^{(0)}}{\partial x_i} + \frac{\partial u_i^{(0)}}{\partial z},\tag{18}$$

with counterpart equations for material B in Ω_B .

We seek to make analytical progress by exploiting linearity of the equations for stress (17), (18), enabling us to pose solutions of the form

$$u_k^{A(1)} = W_{Ak}^{ij}(\mathbf{X}) \frac{\partial u_i^{(0)}}{\partial x_i} + V_{Ak}^i(\mathbf{X}) \frac{\partial u_i^{(0)}}{\partial z} + \phi_{Ak}^i(\mathbf{X}) \frac{\partial w^{(0)}}{\partial x_i} + \psi_{Ak}(\mathbf{X}) \frac{\partial w^{(0)}}{\partial z} + \bar{u}_k(\mathbf{x}, z)$$

and

$$w^{A(1)} = \bar{W}_A^{ij}(\mathbf{X}) \frac{\partial u_i^{(0)}}{\partial x_i} + \bar{V}_A^i(\mathbf{X}) \frac{\partial u_i^{(0)}}{\partial z} + \bar{\phi}_A^i(\mathbf{X}) \frac{\partial w^{(0)}}{\partial x_i} + \bar{\psi}_A(\mathbf{X}) \frac{\partial w^{(0)}}{\partial z} + \bar{w}(\mathbf{x}, z).$$

Such ansatzes have been used in the literature to describe analogous 3D multiscale problems, for example in [26,28], introducing 3^3 cell variables per domain. However, the assumption that the interface between A and B is fixed in z (or specifically, fixed to leading order in z) allows us to propose simpler ansatz of the form

$$u_k^{A(1)} = W_{Ak}^{ij}(\mathbf{X}) \frac{\partial u_i^{(0)}}{\partial x_j} + W_{Ak}^0(\mathbf{X}) \frac{\partial w^{(0)}}{\partial z} + \bar{u}_k(\mathbf{x}, z), \tag{19}$$



6 Page 6 of 24 E. A. Doman et al.

and

$$w^{A(1)} = \phi_A^i(\mathbf{X}) \left(\frac{\partial w^{(0)}}{\partial x_i} + \frac{\partial u_i^{(0)}}{\partial z} \right) + \bar{w}(\mathbf{x}, z). \tag{20}$$

Substituting these ansatz into the system of equations (15)–(18) leads to the following set of three decoupled equations for the unknown variables $W_{\Omega i}^{pq}$, $W_{\Omega i}^{0}$ and ϕ_{Ω}^{p} that make up the microscale cell problem: For $W_{\Omega i}^{pq}$:

$$(1 + \alpha_A) \frac{\partial^2 W_{\Omega i}^{pq}}{\partial X_k \partial X_i} + \frac{\partial^2 W_{\Omega k}^{pq}}{\partial X_i \partial X_i} = 0 \quad \text{for } \Omega = A, \text{ or } B,$$
(21)

$$W_{Ak}^{pq} = W_{Bk}^{pq} \quad \text{on } \Gamma, \tag{22}$$

$$n_{j}\left(\mu\alpha_{A}\frac{\partial W_{Ak}^{pq}}{\partial X_{k}}-\alpha_{B}\frac{\partial W_{Bk}^{pq}}{\partial X_{k}}\right)+n_{j}(\mu\alpha_{A}-\alpha_{B})\delta_{pq}+\mu n_{i}\left(\frac{\partial W_{Ai}^{pq}}{\partial X_{j}}+\frac{\partial W_{Aj}^{pq}}{\partial X_{i}}\right)$$

$$-n_i \left(\frac{\partial W_{Bi}^{pq}}{\partial X_j} + \frac{\partial W_{Bj}^{pq}}{\partial X_i} \right) + n_i (\mu - 1) (\delta_{ip} \delta_{jq} + \delta_{iq} \delta_{jp}) = 0 \quad \text{on } \Gamma.$$
 (23)

For $W_{\Omega i}^0$:

$$(1 + \alpha_A) \frac{\partial^2 W_{\Omega i}^0}{\partial X_k \partial X_i} + \frac{\partial^2 W_{\Omega k}^0}{\partial X_i \partial X_i} = 0 \quad \text{for } \Omega = A, \text{ or } B,$$
(24)

$$W_{Ak}^0 = W_{Rk}^0 \quad \text{on } \Gamma, \tag{25}$$

$$n_{j}\left(\mu\alpha_{A}\frac{\partial W_{Ak}^{0}}{\partial X_{k}}-\alpha_{B}\frac{\partial W_{Bk}^{0}}{\partial X_{k}}\right)+n_{j}(\mu\alpha_{A}-\alpha_{B})$$

$$+ \mu n_i \left(\frac{\partial W_{Ai}^0}{\partial X_j} + \frac{\partial W_{Aj}^0}{\partial X_i} \right) - n_i \left(\frac{\partial W_{Bi}^0}{\partial X_j} + \frac{\partial W_{Bj}^0}{\partial X_i} \right) = 0 \quad \text{on } \Gamma.$$
 (26)

For ϕ_{Ω}^{p} :

$$\frac{\partial^2 \phi_{\Omega}^p}{\partial X_i \partial X_i} = 0 \quad \text{for } \Omega = A, \text{ or } B, \tag{27}$$

$$\phi_A^P = \phi_B^P \quad \text{on } \Gamma, \tag{28}$$

$$n_i \left(\mu \frac{\partial \phi_A^p}{\partial X_i} - \frac{\partial \phi_B^p}{\partial X_i} \right) + n_p(\mu - 1) = 0 \quad \text{on } \Gamma.$$
 (29)

Note that, due to the form of the ansatzes (19), (20) and periodicity on the microscale, the average of the barred terms $\bar{\bf u}$ and $\bar{\bf w}$ is zero across the cell. Additionally, due to the symmetry of the jump in (23) we note that $W_{Ak}^{pq} = W_{Ak}^{qp}$ and similarly for B. Once the macroscale geometry is fixed, Eqs. (21)–(29) may be solved to determine the variables $W_{\Omega i}^{pq}$, $W_{\Omega i}^{0}$ and ϕ_{Ω}^{p} , so that the order ϵ correction to the stresses, (17), (18), are known subject to solving for the globally varying displacement fields. Next we move to the order ϵ^2 system to determine the effective macroscale equations to evaluate these fields.



2.3 Deriving the effective macroscale model

In this section, we seek to determine a macroscale model for the leading-order displacement fields $\mathbf{u}^{(0)}$ and $w^{(0)}$, which only vary globally. Equating coefficients of powers of ϵ^2 in the model (7)–(9) subject to expansions of the form (13) yields the system of equations

$$(1 + \alpha_A) \left(\frac{\partial^2 u_i^{A(2)}}{\partial X_k \partial X_i} + \frac{\partial^2 u_i^{A(1)}}{\partial X_k \partial x_i} + \frac{\partial^2 w^{A(1)}}{\partial z \partial X_k} + \frac{\partial^2 u_i^{A(1)}}{\partial x_k \partial X_i} + \frac{\partial^2 u_i^{(0)}}{\partial x_k \partial x_i} + \frac{\partial^2 w^{(0)}}{\partial x_k \partial x_i} + \frac{\partial^2 w^{(0)}}{\partial x_k \partial z} \right) + \frac{\partial^2 u_k^{A(2)}}{\partial X_i \partial X_i} + 2 \frac{\partial^2 u_k^{A(1)}}{\partial X_i \partial x_i} + \frac{\partial^2 u_k^{(0)}}{\partial x_i \partial x_i} + \frac{\partial^2 u_k^{(0)}}{\partial z^2} = 0$$
(30)

$$\frac{\partial^2 w^{A(2)}}{\partial X_i \partial X_i} \ + 2 \frac{\partial^2 w^{A(1)}}{\partial X_i \partial x_i} + \frac{\partial^2 w^{(0)}}{\partial x_i \partial x_i}$$

$$+(1+\alpha_A)\left(\frac{\partial^2 u_i^{A(1)}}{\partial z \partial X_i} + \frac{\partial^2 u_i^{(0)}}{\partial z \partial x_i}\right) + (2+\alpha_A)\frac{\partial^2 w^{(0)}}{\partial z^2} = 0,\tag{31}$$

subject to the expected boundary conditions on Γ that

$$u_i^{A(2)} = u_i^{B(2)}, \quad w^{A(2)} = w^{B(2)}, \quad \text{and} \quad \mu \tau_{ij}^{A(2)} n_i = \tau_{ij}^{B(2)} n_i,$$
 (32)

$$\tau_{ij}^{A(2)} = \delta_{ij}\alpha_A \left(\frac{\partial u_k^{A(2)}}{\partial X_k} + \frac{\partial u_k^{A(1)}}{\partial x_k} + \frac{\partial w^{A(1)}}{\partial z} \right) + \frac{\partial u_i^{A(2)}}{\partial X_j} + \frac{\partial u_j^{A(2)}}{\partial X_i} + \frac{\partial u_i^{A(1)}}{\partial x_j} + \frac{\partial u_j^{A(1)}}{\partial x_i}, \tag{33}$$

$$\tau_{i3}^{A(2)} = \frac{\partial w^{A(2)}}{\partial X_i} + \frac{\partial w^{A(1)}}{\partial x_i} + \frac{\partial u_i^{A(1)}}{\partial z},\tag{34}$$

with counterpart equations in material B.

Using the definitions of τ_{ij} and τ_{i3} , the governing equations (30), (31) can be rewritten as

$$\frac{\partial \tau_{ik}^{A(2)}}{\partial X_i} + \frac{\partial^2 u_i^{A(1)}}{\partial X_k \partial x_i} + \frac{\partial^2 w^{A(1)}}{\partial z \partial X_k} + \alpha_A \frac{\partial^2 u_i^{A(1)}}{\partial x_k \partial X_i} + (1 + \alpha_A) \left(\frac{\partial^2 u_i^{(0)}}{\partial x_k \partial x_i} + \frac{\partial^2 w^{(0)}}{\partial x_k \partial z} \right) + \frac{\partial^2 u_k^{A(1)}}{\partial X_i \partial x_i} + \frac{\partial^2 u_k^{(0)}}{\partial x_i \partial x_i} + \frac{\partial^2 u_k^{(0)}}{\partial z^2} = 0,$$
(35)

$$\frac{\partial \tau_{i3}^{A(2)}}{\partial X_i} + \frac{\partial^2 w^{A(1)}}{\partial X_i \partial x_i} + \frac{\partial^2 w^{(0)}}{\partial x_i \partial x_i} + \alpha_A \frac{\partial^2 u_i^{A(1)}}{\partial z \partial X_i} + (1 + \alpha_A) \frac{\partial^2 u_i^{(0)}}{\partial z \partial x_i} + (2 + \alpha_A) \frac{\partial^2 w^{(0)}}{\partial z^2} = 0. \tag{36}$$

Integrating these final two equations over the microcell, and using both the periodicity assumption and boundary conditions (32) to eliminate the second-order terms yields the effective macroscale equations

$$(K_{pqik} + K_{pqki}) \frac{\partial^{2} u_{p}^{(0)}}{\partial x_{q} \partial x_{i}} + (K_{ik}^{0} + K_{ki}^{0}) \frac{\partial^{2} w^{(0)}}{\partial z \partial x_{i}} + H_{pk} \left(\frac{\partial^{2} w^{(0)}}{\partial x_{p} \partial z} + \frac{\partial^{2} u_{p}^{(0)}}{\partial z^{2}} \right)$$

$$+ G_{pq} \frac{\partial^{2} u_{p}^{(0)}}{\partial x_{k} \partial x_{q}} + G^{0} \frac{\partial^{2} w^{(0)}}{\partial x_{p} \partial z} + A_{1} \left(\frac{\partial^{2} u_{i}^{(0)}}{\partial x_{k} \partial x_{i}} + \frac{\partial^{2} w^{(0)}}{\partial z \partial x_{k}} \right) + A_{2} \left(\frac{\partial^{2} u_{k}^{(0)}}{\partial x_{i} \partial x_{i}} + \frac{\partial^{2} u_{k}^{(0)}}{\partial z^{2}} \right) = 0,$$

$$(37)$$

$$H_{pi}\left(\frac{\partial^2 w^{(0)}}{\partial x_p \partial x_i} + \frac{\partial^2 u_p^{(0)}}{\partial z \partial x_i}\right) + A_2 \frac{\partial^2 w^{(0)}}{\partial x_i \partial x_i} + G_{pq} \frac{\partial^2 u_p^{(0)}}{\partial x_q \partial z} + G^0 \frac{\partial^2 w^{(0)}}{\partial z^2}$$

$$+ A_1 \frac{\partial^2 u_i^{(0)}}{\partial z \partial x_i} + (A_1 + A_2) \frac{\partial^2 w^{(0)}}{\partial z^2} = 0,$$

$$(38)$$



6 Page 8 of 24 E. A. Doman et al.

where

$$K_{pqki} = \mu \iint_{\Omega_A} \frac{\partial W_{Ak}^{pq}}{\partial X_i} \, \mathrm{d}A + \iint_{\Omega_B} \frac{\partial W_{Bk}^{pq}}{\partial X_i} \, \mathrm{d}A,\tag{39}$$

$$K_{ik}^{0} = \mu \iint_{\Omega_{A}} \frac{\partial W_{Ak}^{0}}{\partial X_{i}} \, \mathrm{d}A + \iint_{\Omega_{B}} \frac{\partial W_{Bk}^{0}}{\partial X_{i}} \, \mathrm{d}A,\tag{40}$$

$$H_{pk} = \mu \iint_{\Omega_A} \frac{\partial \phi_A^p}{\partial X_k} dA + \iint_{\Omega_B} \frac{\partial \phi_B^p}{\partial X_k} dA, \tag{41}$$

$$G_{pq} = \mu \alpha_A \iint_{\Omega_A} \frac{\partial W_{Ai}^{pq}}{\partial X_i} dA + \alpha_B \iint_{\Omega_B} \frac{\partial W_{Bi}^{pq}}{\partial X_i} dA, \tag{42}$$

$$G^{0} = \mu \alpha_{A} \iint_{\Omega_{A}} \frac{\partial W_{Ai}^{0}}{\partial X_{i}} dA + \alpha_{B} \iint_{\Omega_{B}} \frac{\partial W_{Bi}^{0}}{\partial X_{i}} dA, \tag{43}$$

$$A_1 = (1 + \alpha_A)\mu |\Omega_A| + (1 + \alpha_B)|\Omega_B|, \tag{44}$$

and

$$A_2 = \mu |\Omega_A| + |\Omega_B|. \tag{45}$$

Due to the symmetry in the microscale jump condition (23) we can see that $W_{\Omega i}^{pq} = W_{\Omega i}^{qp}$ meaning that several symmetries in these constants can be specified, namely $K_{pqki} = K_{qpki}$ and $G_{pq} = G_{qp}$.

Equations (37), (38) represent the leading-order effective model on the macroscale. They incorporate the impact of the microscale geometry and mechanics on this macroscale behaviour, explicitly through the tensors (39)–(43), and constants (44)–(45), which both represent averages over different microscale parameters and variables. Indeed, once the microscale geometry is fixed, the microscale variables W and ϕ can be determined by solving the microscale problems (21)–(29), and subsequently averaged to evaluate the tensors K, G and H, noting that the other constants (44), (45) are simply related to the microscale geometry. It is then possible to solve Eqs. (37), (38) solely on the macroscale geometry, subject to appropriate macroscale boundary conditions.

2.4 Implementing the SAH model

Having developed an effective model for the macroscale mechanical response of a linearly elastic fibre-supported composite material, we seek to explore the SAH model behaviour by solving it under typical macroscale geometries and loading conditions. In this section, the computational procedure required to implement the SAH Model is presented, alongside a demonstration of the multiscale model behaviour.

The analysis so far is applicable to any fibre-supported structure with an identifiable periodic microstructure. Composite materials of this family are called *monoclinic*—a class of anisotropic materials with three distinct orthogonal axis and a single plane of symmetry [35] (which we have taken to be in the x-y plane). To implement this model effectively, a further assumption is made that the microscale cell is regular with both symmetric and rotational symmetry around a single axis, for example, as in Fig. 2. This allows us to describe the composite material as a *transversely isotropic material* enabling us to use standard results in our computational implementation, such as those in [36], for example.

As an example, simulations of the macroscale model (37), (38) are carried out on a cylindrical geometry, the microscale cross-section of which is shown in Fig. 2. Rewriting the macroscale model, (37), (38), in the form

$$\nabla \cdot \tau_{ij}^{\text{eff}} = 0,$$

allows us to identify the effective stress tensors as given in Appendix A. This, in turn, enables us to use the generalised Hookes' Law

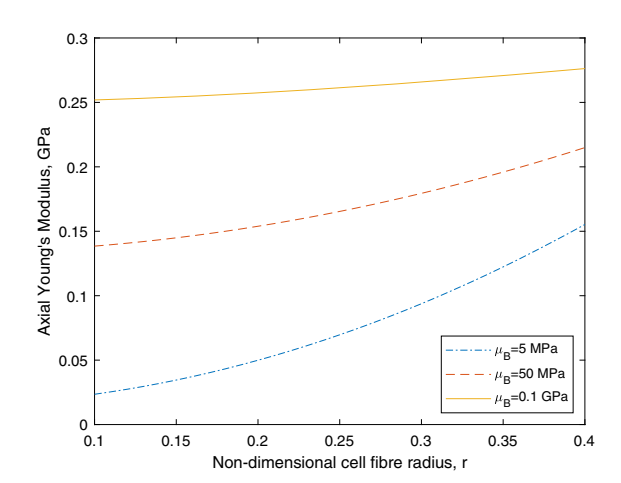
$$\tau_{ij}^{\text{eff}} = c_{ijkl} \epsilon_{kl},$$



Fig. 2 Example microscale geometry where Ω_A and Ω_B are the areas containing materials A and B, respectively. The non-dimensional cell fibre radius is denoted by r

 Ω_B Γ Ω_A

Fig. 3 Simulation results from the macroscale model (37), (38) showing the Young's Modulus of the homogenised material as a function of the non-dimensional cell fibre radius r, see Fig. 2. Material parameters are set to $\mu_A = 0.1$ GPa, $\lambda_A = 1.5$ GPA, $\lambda_B = 0.1$ GPa and μ_B is varied



where ϵ_{kl} is the effective strain, and to express the elasticity tensor c_{ijkl} entirely in terms of the microscale variables (39)–(45). Using standard linear elasticity assumptions, it is convenient to contract the fourth-rank elasticity tensor to the second-order Voigt or Engineering notation tensor C_{ij} , [35] and, thus, express C_{ij} in terms of the microscale variables (39)–(45) as given in Appendix B. Given that the rudimentary geometry under consideration is transversely isotropic, it can be shown [36] that the axial Poisson ratio is given by

$$\nu = \frac{C_{13}}{C_{11} + C_{12}},\tag{46}$$

and the non-dimensional axial Young's Modulus can be expressed as

$$E = \frac{C_{11}C_{33} - 2C_{13}^2 + C_{33}C_{12}}{C_{11} + C_{12}}. (47)$$

The Young's Modulus may be redimensionalised using μ_B , consistent with the definition of μ in Sect. 2.1.

The significant computational effort in this case, therefore, is to determine the averaged microscale parameters (39)–(45) in the microscale geometry. COMSOL Multiphysics, a finite element software, is used to conduct the simulations given its flexibility for solving complex PDEs in different geometries. The three microscale systems of equations (21)–(29) are solved for the specified 2D microscale cell geometry, given in Fig. 2, and the averaged microscale parameters (39)–(45) are determined for varying ranges of microscale mechanical properties and geometric variables. This, in turn, allows us to explore the impact of the microscale parameters on the effective macroscale predictions using formulae (46), (47). Some example plots are presented in Fig. 3, showing, as expected, that axial Young's Moduli increases as the proportion of stiffer material increases in the composite material, and this occurs at different rates dependent on the shear moduli.



6 Page 10 of 24 E. A. Doman et al.

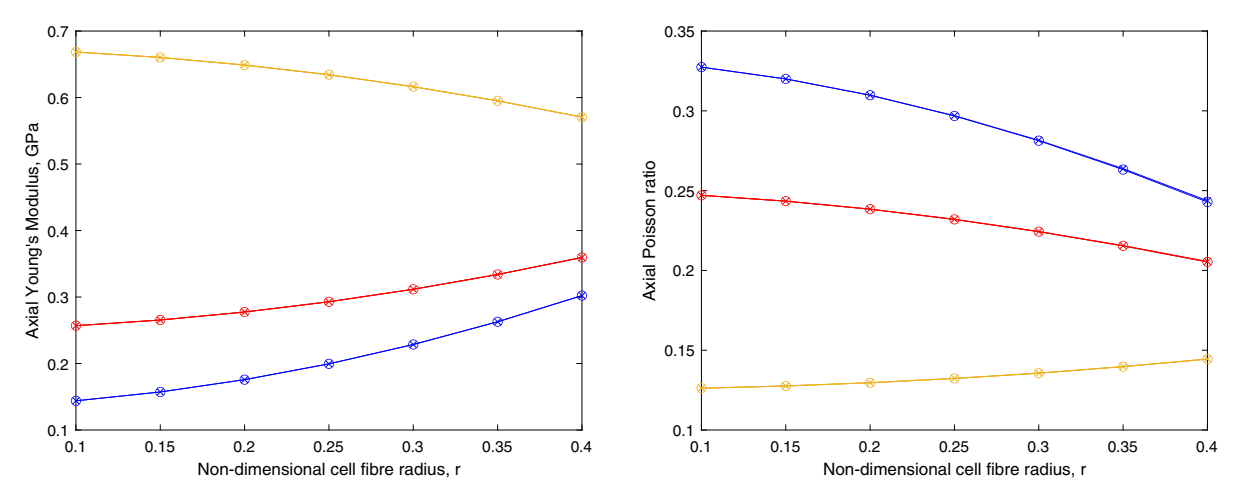


Fig. 4 Comparison between macroscale model (37), (38), denoted by solid line and other elastic homogenisation models developed by Parnell and Abrahams, [26], denoted by starred line, and Penta and Gerisch, [27], denoted by line with circles. Non-dimensional cell fibre radius, r is varied with $\mu_A = 0.2$ GPa and $\lambda_A = \lambda_B = 0.1$ GPa, and $\mu_B = 0.05$ (blue), 0.1 (red) or 0.3 (yellow) GPa. (Color figure online)

Figure 4 shows a comparison between the model derived in this paper and two recent homogenisation models [26,27]. For all three models the axial Young's Moduli and Poisson ratios vary dependent on the proportion of stiffer material present in the composite material. Our model is consistent with the values obtained from the other two models as would be expected, as the same constitutive equations have been adopted. In the next two sections, we explore how the model can be modified to deal with different assumptions on the microscale behaviour by taking various limits in the material properties.

3 Compressible-incompressible interaction model

Incompressibility is a common assumption made of the mechanical properties of many materials. This is, of course, an approximation as many materials relevant to the tissue engineering community have a large bulk modulus in reality, but are not absolutely incompressible [37,38]. In this section, we explore how the model developed in Sect. 2 can be adapted to account for an incompressible component in the composite material. Primarily, this involves a different formulation of the microscale mechanical model, due to the differing constitutive equations on the microscale. Without loss of generality we have chosen to set the inner material A to be incompressible, noting that the analysis would follow similarly if the outer material B was chosen to be incompressible instead.

The analysis follows that of the SAH model given in Sect. 2, except that in material A, instead of using (1), (2), we use the incompressible linearly elastic Navier equations, which are given by

$$-\frac{\partial p^*}{\partial X_k^*} + \mu_A \left(\frac{\partial^2 u_k^{A*}}{\partial X_i^* \partial X_i^*} + \frac{\partial^2 u_k^{A*}}{\partial z^{*2}} \right) = 0, \tag{48}$$

$$-\frac{\partial p^*}{\partial z^*} + \mu_A \left(\frac{\partial^2 w^{A*}}{\partial X_i^* \partial X_i^*} + \frac{\partial^2 w^{A*}}{\partial z^{*2}} \right) = 0, \tag{49}$$

and

$$\frac{\partial u_k^{A*}}{\partial X_k^*} + \frac{\partial w^{A*}}{\partial z^*} = 0,\tag{50}$$

where p^* is the non-dimensional pressure in A. The same non-dimensionalise scalings (6) as in Sect. 2 are adopted, but with the addition of the unknown isotropic unknown pressure which is scaled $p^* = Pp + p_0$ where p_0 is atmospheric pressure.



Note, as in the compressible–compressible case, the stress tensor scaling $\tau_{ij}^{B*} = \mu_B \epsilon^{-1} \tau_{ij}^{B}$ is used and therefore, to ensure continuity of stress on the interface Γ between the two materials, we must take $\tau_{ij}^{A*} = \mu_A \epsilon^{-1} \tau_{ij}^A$. Moreover, assuming that the pressure in the incompressible material can potentially contribute to the leading-order effective composite stress, the scaling $P = \mu_A \epsilon^{-1}$ is assumed. As before $\epsilon = \frac{\delta}{d}$, $\mu = \frac{\mu_A}{\mu_B}$ and $\alpha_B = \frac{\lambda_B}{\mu_B}$. As in the general case, we assume μ , $\alpha_{A,B}$ and $\beta_{A,B}$ to be of order unity and the non-dimensional equations in Ω_A are now

$$-\frac{\partial p}{\partial X_k} + \frac{\partial^2 u_k^A}{\partial X_i \partial X_i} + \epsilon^2 \frac{\partial^2 u_k^A}{\partial z^2} = 0, \tag{51}$$

$$-\epsilon \frac{\partial p}{\partial z} + \frac{\partial^2 w^A}{\partial X_i \partial X_i} + \epsilon^2 \frac{\partial^2 w^A}{\partial z^2} = 0, \tag{52}$$

$$\frac{\partial u_k^A}{\partial X_k} + \epsilon \frac{\partial w^A}{\partial z} = 0. \tag{53}$$

In Ω_B the non-dimensional equations are

$$(1 + \alpha_B) \left(\frac{\partial^2 u_i^B}{\partial X_k \partial X_i} + \epsilon \frac{\partial^2 w^B}{\partial X_k \partial z} \right) + \frac{\partial^2 u_k^B}{\partial X_i \partial X_i} + \epsilon^2 \frac{\partial^2 u_k^B}{\partial z^2} = 0, \tag{54}$$

and

$$(1 + \alpha_B) \left(\epsilon \frac{\partial^2 u_i^B}{\partial z \partial X_i} + \epsilon^2 \frac{\partial^2 w^B}{\partial z^2} \right) + \frac{\partial^2 w^B}{\partial X_i \partial X_i} + \epsilon^2 \frac{\partial^2 w^B}{\partial z^2} = 0.$$
 (55)

The same usual conditions of continuity of displacement and stress, (9), are applied at the interface Γ between the two materials, but note that now

$$\tau_{ij}^{A} = -p\delta_{ij} + \frac{\partial u_{i}^{A}}{\partial X_{i}} + \frac{\partial u_{j}^{A}}{\partial X_{i}} \quad \text{and} \quad \tau_{i3}^{A} = \frac{\partial w^{A}}{\partial X_{i}} + \epsilon \frac{\partial u_{i}^{A}}{\partial z}. \tag{56}$$

As utilised in Sect. 2, we introduce the macroscale coefficient $x_k = \epsilon X_k$ and equate coefficients of ϵ^0 in equations (51)–(55) and in the boundary conditions (9) on Γ . Then leading-order solution is identical to the general case as expected with the addition requirement that $p^{(0)} = p^{(0)}(\mathbf{x}, z)$. The continuity of stress boundary condition reduces this to $p^{(0)} = 0$ on Γ and, hence, we require $p^{(0)} = 0$ for all **x** and z. Leading-order variations in incompressible pressure, therefore, only occur on the microscale.

3.1 Microscale problem

By equating coefficients of ϵ^1 in Eqs. (51)–(55) and boundary conditions (9), we obtain the counterparts of Eqs. (15) for material B (with incompressible version for A) that define the microscale cell problem. The same ansatzes, (19), (20), as the general case applies, but an additional expression of the form

$$p^{(1)} = P^{1}(\mathbf{X}) \frac{\partial u^{(0)}}{\partial x} + P^{2}(\mathbf{X}) \frac{\partial v^{(0)}}{\partial y} + Q(\mathbf{X}) \frac{\partial w^{(0)}}{\partial z}$$

$$(57)$$

is included to account for the isotropic pressure term in material A. These ansatzes allow us to consider coefficients of macroscale derivatives and so formulate the cell problem solely in terms of the microscale. This microscale cell problem again conveniently uncouples into three systems as in (21)–(29) that may be stated separately as follows:

$$\frac{\partial^2 W_{Ak}^{pq}}{\partial X_i \partial X_i} = \begin{cases} \frac{\partial P^p}{\partial X_k} & \text{when } p = q, \\ 0 & \text{otherwise} \end{cases} \quad \text{and} \quad \frac{\partial W_{Ak}^{pq}}{\partial X_k} + \delta_{pq} = 0 \quad \text{on } \Omega_A,$$
 (58)

$$(1 + \alpha_B) \frac{\partial^2 W_{Bi}^{pq}}{\partial X_k \partial X_i} + \frac{\partial^2 W_{Bk}^{pq}}{\partial X_i \partial X_i} = 0 \quad \text{on } \Omega_B,$$
(59)



6 Page 12 of 24 E. A. Doman et al.

with boundary conditions on Γ that $W_{Ak}^{pq} = W_{Bk}^{pq}$, as before, and

$$\alpha_{B}n_{j}\left(\frac{\partial W_{Bk}^{pq}}{\partial X_{k}} + \delta_{pq}\right) + n_{i}\left(\frac{\partial W_{Bi}^{pq}}{\partial X_{j}} + \frac{\partial W_{Bj}^{pq}}{\partial X_{i}}\right) + n_{i}(\delta_{ip}\delta_{jq} + \delta_{jp}\delta_{iq})$$

$$= n_{i}\mu\left(\frac{\partial W_{Ai}^{pq}}{\partial X_{j}} + \frac{\partial W_{Aj}^{pq}}{\partial X_{i}}\right) + n_{i}\mu(\delta_{ip}\delta_{jq} + \delta_{jp}\delta_{iq}) + \begin{cases} -P^{p}\mu n_{j} & \text{when } p = q, \\ 0 & \text{otherwise.} \end{cases}$$
(60)

For $W_{\Omega i}^0$:

$$\frac{\partial^2 W_{Ak}^0}{\partial X_i \partial X_i} = \frac{\partial Q}{\partial X_k} \quad \text{and} \quad \frac{\partial W_{Ak}^0}{\partial X_k} + 1 = 0 \quad \text{on } \Omega_A, \tag{61}$$

$$(1 + \alpha_B) \frac{\partial^2 W_{Bi}^0}{\partial X_k \partial X_i} + \frac{\partial^2 W_{Bk}^0}{\partial X_i \partial X_i} = 0 \quad \text{on } \Omega_B,$$
(62)

with boundary conditions on Γ that $W_{Ai}^0=W_{Bi}^0$ as before and

$$\alpha_B n_j \left(\frac{\partial W_{Bk}^0}{\partial X_k} + 1 \right) + n_i \left(\frac{\partial W_{Bi}^0}{\partial X_j} + \frac{\partial W_{Bj}^0}{\partial X_i} \right) = -n_j \mu Q + n_i \mu \left(\frac{\partial W_{Ai}^0}{\partial X_j} + \frac{\partial W_{Aj}^0}{\partial X_i} \right). \tag{63}$$

For ϕ_{Ω}^{p} :

this system of ϕ_{Ω}^{p} is identical to Eqs. (27)–(29) in the general case.

3.2 Deriving the effective macroscale equations

By equating coefficients of ϵ^1 in Eqs. (51)–(55) and boundary conditions (9), and following the same process as in Sect. 2.3 the second-order governing equations are obtained for the compressible–incompressible setup. These equations are further reduced using the coefficients of ϵ in the continuity equation (53) to obtain

$$\frac{\partial \tau_{ik}^{A(2)}}{\partial X_i} + \frac{\partial^2 u_i^{A(1)}}{\partial X_k \partial X_i} + \frac{\partial^2 w^{A(1)}}{\partial X_k \partial z} + \frac{\partial^2 u_i^{(0)}}{\partial x_k \partial x_i} + \frac{\partial^2 w^{(0)}}{\partial x_k \partial z} - \frac{\partial p^{(1)}}{\partial x_k} + \frac{\partial^2 u_k^{A(1)}}{\partial x_i \partial X_i} + \frac{\partial^2 u_k^{(0)}}{\partial x_i \partial x_i} + \frac{\partial^2 u_k^{(0)}}{\partial z^2} = 0,$$
(64)

and

$$\frac{\partial \tau_{i3}^{A(2)}}{\partial X_i} - \frac{\partial p^{(1)}}{\partial z} + \frac{\partial^2 w^{A(1)}}{\partial X_i \partial x_i} + \frac{\partial^2 w^{(0)}}{\partial x_i \partial x_i} + \frac{\partial^2 u_i^{(0)}}{\partial z \partial z_i} + 2\frac{\partial^2 w^{(0)}}{\partial z^2} = 0.$$
 (65)

By integrating over the cell, adding the equations in the two materials, and then using the continuity of stress boundary condition and the Divergence Theorem, we are able to eliminate terms involving second-order variables. From this, we obtain the same homogenised equations (37), (38) as derived in the general case, with the same microscale averaged parameters K_{pqki} , K_{ik}^0 , H_{pk} and A_2 , given by (39)–(41), (44), (45). The incompressibility of material A, however, causes G_{pq} , G^0 and A_1 to be redefined in terms of the isotropic pressure terms of the ansatz as follows:

$$G_{pq} = \alpha_B \iint_{\Omega_B} \frac{\partial W_{Bi}^{pq}}{\partial X_i} dA - \mu \begin{cases} \iint_{\Omega_A} P^p dA & \text{when } p = q, \\ 0 & \text{otherwise,} \end{cases}$$
 (66)

$$G^{0} = \alpha_{B} \iint_{\Omega_{B}} \frac{\partial W_{Bi}^{0}}{\partial X_{i}} dA - \mu \iint_{\Omega_{A}} Q dA, \tag{67}$$

and

$$A_1 = \mu |\Omega_A| + (1 + \alpha_B)|\Omega_B|. \tag{68}$$



3.3 Implementation of the compressible–incompressible model

As the homogenised equations in Sects. 2 and 3 are unchanged, we may use the same macroscale elastic tensors as those given in Appendix B. The setup of the microscale to evaluate the averaged microscale parameters requires modification as described below.

Solving the microscale system of equations, (27)–(29), for ϕ_{Ω}^{p} is trivial to input into COMSOL Multiphysics as described in Sect. 2. Due to the presence of the constraints from the continuity equation, however, the implementation of the other systems is more complex. For solving Eqs. (58)–(60) with p = q and Eqs. (61)–(63), it is helpful to introduce a potential function ψ^{i} for i = 1, 2 or 3 such that

$$W_{A1}^0 = \frac{\partial \psi^3}{\partial X}, \quad W_{A2}^0 = \frac{\partial \psi^3}{\partial Y}, \tag{69}$$

$$W_{A1}^{11} = \frac{\partial \psi^1}{\partial X}, \quad W_{A2}^{11} = \frac{\partial \psi^1}{\partial Y},$$
 (70)

$$W_{A1}^{22} = \frac{\partial \psi^2}{\partial X}, \quad W_{A2}^{22} = \frac{\partial \psi^2}{\partial Y}.$$
 (71)

Without loss of generality, we set that

$$Q = \frac{\partial^2 \psi^3}{\partial X_i \partial X_i} \quad \text{and} \quad P^i = \frac{\partial^2 \psi^i}{\partial X_j \partial X_j}, \tag{72}$$

for i = 1, 2, to ensure that the only equation we need to solve for each ψ^i will be the constraints resulting from the continuity equations in each case.

On the other hand, for Eqs. (58)–(60) where $p \neq q$ we introduce a streamfunction ζ such that

$$W_{A1}^{12} = \frac{\partial \xi^1}{\partial Y}, \quad W_{A2}^{12} = -\frac{\partial \xi^1}{\partial X}, \quad W_{A1}^{21} = \frac{\partial \xi^2}{\partial Y}, \quad \text{and} \quad W_{A2}^{21} = -\frac{\partial \xi^2}{\partial X},$$
 (73)

that satisfies the constraints resulting from the continuity equation and leaves us with the two remaining governing equations to solve for ξ and the pressure variable in each case.

4 Other physically-relevant limiting behaviours

The previous section investigates the case of an incompressible inner material which can be physically interpreted as the limit of large α_A . In this section, we consider other relevant limiting behaviours of the model, providing a framework to guide the reader on how to approach any possible combination of parameter regimes. We begin by firstly examining the impact of alternative scalings of μ , the ratio of the shear moduli of the two components of the composite material, before moving onto considering the effect of a highly compressible material by considering small α_A . The results from these limiting models are compared in Sect. 5 with the results of simulations of these differing limiting behaviours using the SAH approach presented in Sect. 2.

4.1 Varying the ratio of the shear moduli

We first consider the effect of varying the size of μ , the ratio of the shear moduli of the two materials making up the composite material. As μ only appears in the boundary condition (9), this means that in taking the large or small limit of μ we are effectively decoupling the stresses in the two materials. It is worth noting, therefore, that large and small limits of μ have symmetric effects on the theoretical model. Here, the approach taken when μ is large is presented along and with comments on the differences that occur when considering μ small.



Page 14 of 24 E. A. Doman et al.

Again the same non-dimensionalisation and model setup is used as in Sect. 2, except that we impose the scaling $\mu = \epsilon^{-1}\bar{\mu}$, where $\bar{\mu} \sim \mathcal{O}(1)$. The stress continuity boundary condition (9) becomes

$$\bar{\mu}\tau_{ij}^{A(0)}n_i = 0 \text{ and } \bar{\mu}\tau_{ij}^{A(k)}n_i = \tau_{ij}^{B(k-1)}n_i,$$
 (74)

for $k \geq 1$ where $\tau_{ij}^{A(k)}$ and $\tau_{ij}^{B(k)}$ are as defined in Sect. 2. The analysis follows as in the SAH Model in Sect. 2, but while the same ansatz holds as before in A, due to the continuity of displacement boundary condition, using the same ansatz for the displacements in B leads to a contradiction. In order to resolve this, displacement boundary conditions of the form $u_i^{B(0)} = P_{ik}(\mathbf{X})u_i^{(0)}$ and $w^{B(0)} = Q(\mathbf{X})w^{(0)}$ are adopted to create the ansatz. The equations then uncouple and allow us to derive a system of equations to be solved in either Ω_A or Ω_B . The complete system of equations obtained for the microcell problem are given in Appendix C.

Using a combination of the order ϵ^2 and ϵ systems, we are able to integrate over the cell and apply the boundary conditions to obtain the resulting homogenised equations:

$$(K_{pqik} + K_{pqki}) \frac{\partial^{2} u_{p}^{(0)}}{\partial x_{i} \partial x_{q}} + (K_{ki}^{0} + K_{ik}^{0}) \frac{\partial^{2} w^{(0)}}{\partial z \partial x_{i}} + H_{ik} \left(\frac{\partial^{2} w^{(0)}}{\partial x_{i} \partial z} + \frac{\partial^{2} u_{i}^{(0)}}{\partial z^{2}} \right)$$

$$+ G_{pq} \frac{\partial^{2} u_{p}^{(0)}}{\partial x_{k} \partial x_{q}} + G^{0} \frac{\partial^{2} w^{(0)}}{\partial z \partial x_{q}} + (\bar{K}_{pik} + \bar{K}_{pki}) \frac{\partial u_{p}^{(0)}}{\partial x_{i}} + \bar{K}_{k}^{0} \frac{\partial w^{(0)}}{\partial z} + \bar{G}_{p} \frac{\partial u_{p}^{(0)}}{\partial x_{k}}$$

$$+ A_{1} \left(\frac{\partial^{2} u_{i}^{(0)}}{\partial x_{k} \partial x_{i}} + \frac{\partial^{2} w^{(0)}}{\partial z \partial x_{k}} \right) + A_{2} \left(\frac{\partial^{2} u_{k}^{(0)}}{\partial x_{i} \partial x_{i}} + \frac{\partial^{2} u_{k}^{(0)}}{\partial z^{2}} \right) = 0$$

$$(75)$$

and

$$H_{pi}\left(\frac{\partial^{2}w^{(0)}}{\partial x_{p}\partial x_{i}} + \frac{\partial^{2}u_{p}^{(0)}}{\partial x_{i}\partial z}\right) + (K_{kqii} + G_{pq})\frac{\partial^{2}u_{p}^{(0)}}{\partial x_{q}\partial z} + (G^{0} + K_{ii}^{0})\frac{\partial^{2}w^{(0)}}{\partial z^{2}} + \bar{K}_{i}^{0}\frac{\partial w^{(0)}}{\partial x_{i}} + \bar{G}_{p}\frac{\partial u_{p}^{(0)}}{\partial z} + A_{2}\frac{\partial^{2}w^{(0)}}{\partial x_{i}\partial x_{i}} + A_{1}\frac{\partial^{2}u_{i}^{(0)}}{\partial z\partial x_{i}} + (A_{1} + A_{2})\frac{\partial^{2}w^{(0)}}{\partial z^{2}} = 0,$$

$$(76)$$

where

$$A_1 = \bar{\mu}|\Omega_A|(1+\alpha_A), \quad A_2 = \bar{\mu}|\Omega_A|, \quad A_3 = \beta_A\bar{\mu}|\Omega_A|,$$
 (77)

$$K_{pqki} = \bar{\mu} \iint_{\Omega_A} \frac{\partial W_{Ak}^{pq}}{\partial X_i} dA, \quad K_{ik}^0 = \bar{\mu} \iint_{\Omega_A} \frac{\partial W_{Ak}^0}{\partial X_i} dA, \quad H_{pk} = \bar{\mu} \iint_{\Omega_A} \frac{\partial \phi_A^p}{\partial X_k} dA, \tag{78}$$

$$G_{pq} = \bar{\mu}\alpha_A \iint_{\Omega_A} \frac{\partial W_{Ai}^{pq}}{\partial X_i} dA \quad \text{and} \quad G^0 = \bar{\mu}\alpha_A \iint_{\Omega_A} \frac{\partial W_{Ai}^0}{\partial X_i} dA.$$
 (79)

The following terms with bars are not seen in the general case of Sect. 2:

$$\bar{K}_{pik} = \iint_{\Omega_B} \frac{\partial P_{pi}}{\partial X_k} \, dA, \quad \bar{K}_k^0 = \iint_{\Omega_B} \frac{\partial Q}{\partial X_k} \, dA$$
(80)

$$\bar{G}_p = \alpha_B \iint_{\Omega_B} \frac{\partial P_{pi}}{\partial X_i} \, \mathrm{d}A. \tag{81}$$

These new terms are due to the effective softening of the outer material in the analytical work resulting in terms from the previous order contributing to the effect of material B in the homogenised equations.

In the case of μ small, i.e. $\mu = \epsilon \bar{\mu}$ where $\bar{\mu} \sim \mathcal{O}(1)$, this will be analogous to taking material A, to leading order, to be a void. Computationally it would effectively be the similar to the μ large case, but with labels for materials A and B being swapped (with $\bar{\mu}$ still attached to the material A terms).



4.2 Considering highly compressible interactions

In Sect. 3, we considered the effect of the assumption incompressibility in one of the components of the composite material, here we very briefly consider the opposite extreme where one material is highly compressible. We begin by making a re-scaling of $\alpha_A = \epsilon \bar{\alpha}_A$ where $\bar{\alpha}_A \sim \mathcal{O}(1)$. Following through the standard homogenisation procedure with the same scalings and ansatz as in the SAH model shown in Sect. 2, the same homogenised equations, (37), (38), are obtained but the following averaged microscale parameters are redefined:

$$G_{pq} = \alpha_B \iint_{\Omega_B} \frac{\partial W_{Bi}^{pq}}{\partial X_i} dA, \quad G^0 = \alpha_B \iint_{\Omega_B} \frac{\partial W_{Bi}^0}{\partial X_i} dA$$
 (82)

and

$$A_1 = \mu |\Omega_A| + (1 + \alpha_B) |\Omega_B|. \tag{83}$$

5 Comparison with the SAH model

So far, we have described the analytical and computational procedure using asymptotic homogenisation to investigate the effective mechanical properties of fibre-supported composite materials. The semi-analytic SAH Model of a linearly elastic fibre-reinforced composite material, which agrees well with previous models in the literature, is derived in Sect. 2. We then proceeded to adapt the homogenisation procedure to incorporate the mechanical effects of differing extreme limits in the micromechanical properties of the composite material. In this section, we numerically compare the general and limiting models and offer explanations for the discrepancies observed in the obtained results.

Figure 5 shows the limits of axial Young's Modulus predicted by the small and large μ models which correspond well with the values obtained by simulations of the SAH model. Such consistency is to be expected as the averaged microscale parameters (77)–(81) can be obtained straightforwardly by taking the limits of μ large and small in the SAH averaged microscale parameters (39)–(45).

More interestingly, however, is the comparison of axial Poisson ration values in the small and large μ limits, shown in Fig. 6. Here, we see that the SAH Model matches the small limit but does not converge to the large limit. This can be explained by considering the consequences of uncoupling the boundary conditions when taking extreme limits of μ . The small and large limits directly correspond to the axial Poisson ratios of material A (the large limit) and material B (the small limit). When μ is small the Poisson ratio of the material A is also small and the composite material reacts as if material A is a void matching the Poisson ratio of material B. As μ grows the contribution to the Poisson ratio also increases but plateaus at the area-weighted average between the two Poisson ratios. This limit is different to that of the Poisson ratio of material A and leads to discrepancies between the large μ limit and the SAH solution.

Turning now to cases where α_A is varied from very small (highly compressible limit) to very large (incompressible limit) the discrepancy in agreement now occurs both the calculation of the effective axial Young's Modulus and the calculation of effective axial Poisson ratio, see Figs. 7 and 8. The figures consistently show that the small α limit trend is consistent with the Standard Asymptotic Homogenised Model for both the axial Young's Moduli and Poisson ratios, but the incompressible limit ($\alpha_A \ll 1$) differs. The small α limit can be expected to match the SAH model as the effective equations are the same as those in the SAH model, (37), (38). When α_A is small, material A softens and contributes less to the effective mechanical properties, resulting in the revised averaged microscale parameters (82), (83) and the resulting limit obtained in the SAH model.

However, when we consider the compressible–incompressible limit in Figs. 7 and 8, we see a very different limit to that exhibited by the SAH model as α_A becomes large. Both the compressible–incompressible model and the SAH model have the same effective macroscale equations, (37), (38), but the behaviour of the microscale solutions varies markedly. This is due to the additional constraint of continuity equation (50) and the variable the isotropic pressure p^* in Eqs. (48), (49). These additions follow through into the microscale cell problem (58), (61) and add



6 Page 16 of 24 E. A. Doman et al.

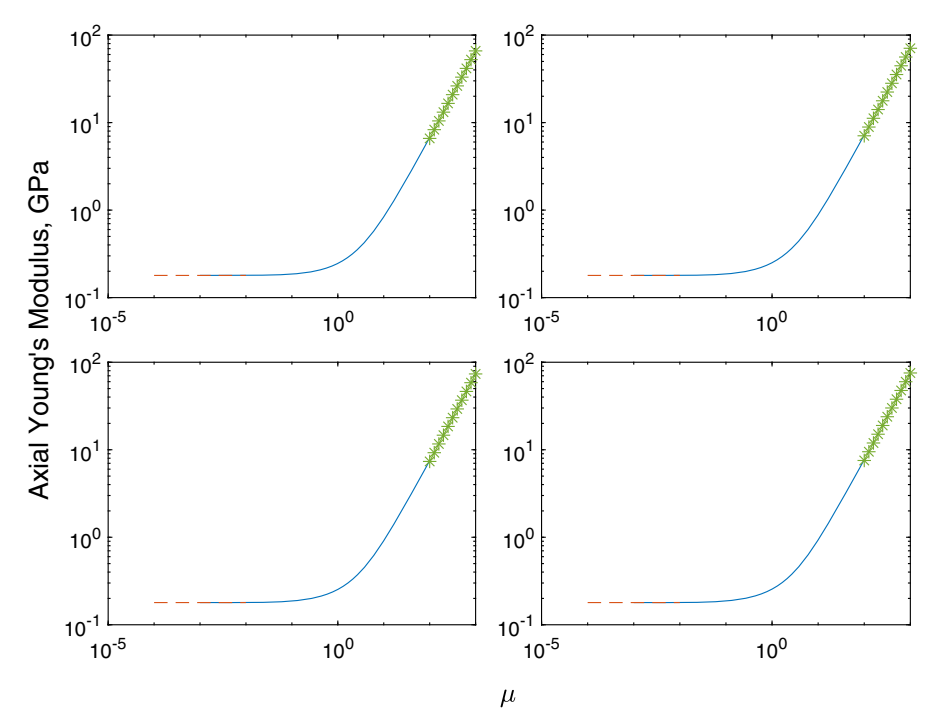


Fig. 5 Plots using simulations of the SAH model described in Sect. 2, small μ and large μ , described in Sect. 4.1, for a range of micromechanical properties to demonstrate that simulations for small and large simulations are the limits of the axial Young's Modulus as given by the general model. Solid blue line shows results from the SAH model. Dashed red line denotes small μ simulation and green stars denote large μ simulation. Micromechanical properties are set to $\mu_A = \mu \mu_B$, $\mu_B = \lambda_B = 0.1$ GPa and $\lambda_A = 0.5 \mu_A$ (top left), μ_A (top right), 1.5 μ_A (bottom left) or 2 μ_A (bottom right). (Color figure online)

additional terms to the respective cell boundary conditions (60), (63). This ultimately results in revised expressions for G_{pq} (66), G^0 (67) and A_1 (68) which are independent of α_A . Such expressions lie in stark contrast to the same tensors for the SAH model (42)–(44) which are linear in α_A and grow unbounded as α_A increases, resulting in the differing limits in the effective macroscale axial Poisson ratio and Young's Moduli. The observed discrepancy between the two models ultimately stems from how we interpret the incompressible limit. A material categorised as incompressible, by considering the effective mechanical properties of the material, must have a Poisson ratio of 0.5. We can write the Poisson ratio of a given material i in terms of the ratio of the Lamé parameters, α_i of that material

$$\nu_i = \frac{1}{2(1 + \frac{1}{\alpha_i})}. (84)$$

Using Eq. (84), we infer that the condition of $v_i = 0.5$ is equivalent to α_i tending to infinity. This would suggest that taking the general model in the limit $\alpha_A \to \infty$ should be equivalent to the compressible–incompressible model. To obtain the incompressible governing equations (48)–(50), however, more stringent limits are conventionally taken, [39], namely that

$$p = \lim_{\epsilon \to 0} -\frac{\mu_i}{\epsilon} \nabla \cdot \mathbf{u},\tag{85}$$

where $\alpha_i = \frac{1}{\epsilon}$, for a nearly incompressible material, leading to the inconsistent trends observed in Figs. (7, 8).



Fig. 6 Plots using simulations of the SAH model described in Sect. 2, small μ and large μ , described in Sect. 4.1, for a range of micromechancial properties to show that the small and large limits of the axial Poisson ratio do not match those of the general case. Solid blue line shows results from SAH model. Dashed red line denotes small μ simulation and green stars denote large μ simulation. Micromechanical properties are set to $\mu_A = \mu \mu_B$, $\mu_B = \lambda_B = 0.1$ GPa and $\lambda_A = 0.5 \mu_A$ (top left), μ_A (top right), 1.5 μ_A (bottom left) or $2\mu_A$ (bottom right). (Color figure online)

6 Discussion and conclusion

A series of 3D fibre-reinforced composite elastic models, valid for various material parameter regimes, has been presented. By separating the microscale and macroscale problems using asymptotic homogenisation, we are able to derive new effective descriptions for the mechanical behaviour of fibre-supported composite materials, which encode information on the microscale geometry and mechanics. Our parallel fibre approach reduces the complexity of the homogenisation procedure for composite materials. However, this approach ultimately requires an understanding of the intrinsic microscale mechanical properties of the composite material in relation to the overall geometry information which is not always available in the current literature.

Throughout this paper, our computational results have shown how different microscale conditions change the macroscopic behaviour of the material. Such a model is likely to be of interest to a range of different industries interested in optimising the mechanical behaviour of composite materials.

Our results are built on the SAH derived in Sect. 2, a model which is analogous to other similar models in the literature, but can also be adapted to account for a broader range of microscale behavioural limits. The key contribution of this work is highlighting how uncertainty in the micromechancial properties of a composite material can potentially translate to different predictions of the effective mechanical properties, depending on the microscale assumptions made in the homogenisation process. For instance, when considering the small and large limits of the ratio of shear moduli in a composite material (Figs. 5, 6), discrepancies in the calculated effective Poisson's Ratio are observed in the case of a large difference in shear moduli, where homogenisation models constructed using different microscale assumptions produce different values. Despite this, the calculated effective Young's Moduli remained consistent. The discrepancies in this case are due to the fact that the models constructed assuming the extreme limits of this ratio weigh the mechanical contributions of each material differently than the SAH homogenisation setup.



6 Page 18 of 24 E. A. Doman et al.

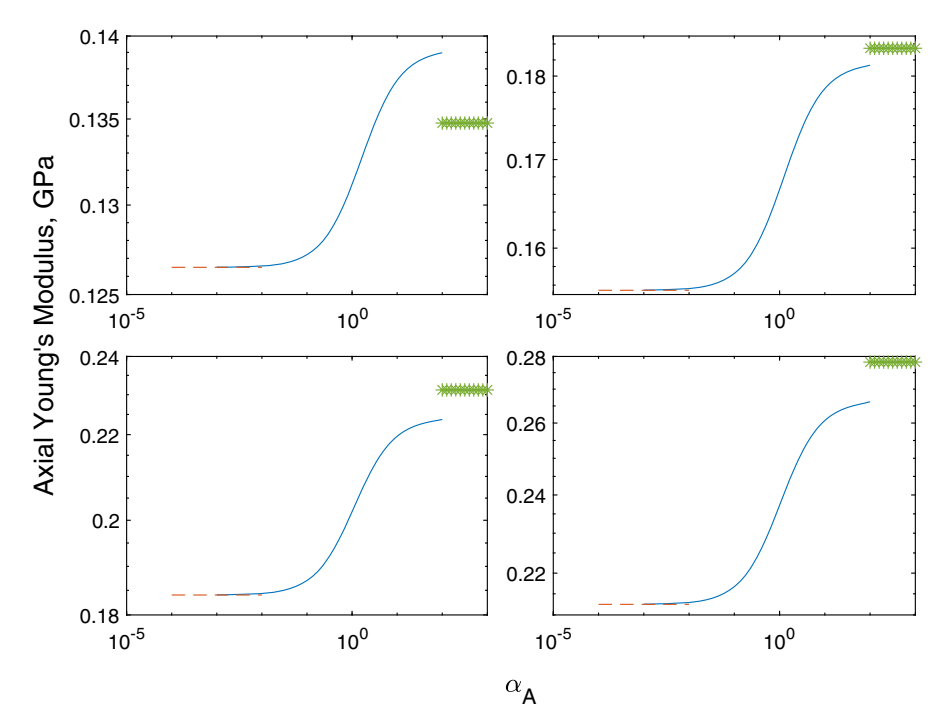


Fig. 7 Plots using simulations of SAH model described in Sect. 2, small μ and large μ , described in Sect. 4.1, for a range of micromechancial properties to show that the small and large limits of the axial Young's Modulus do not match those of the SAH model. Dashed red line denotes small μ simulation and green stars denote large μ simulation. Micromechanical properties are set to $\mu_B = 50$ MPa, $\lambda_B = 0.1$ GPa and $\lambda_A = \alpha_A \mu_A$, where $\mu_A = 50$ MPa (top left), 0.1 GPa (top right), 0.15 GPa (bottom left) or 0.2 GPa (bottom right). (Color figure online)

Hence, for a composite material where there is likely to be an extreme difference in shear moduli, our analysis suggests care must be taken in using an asymptotic homogenised model to determine the effective macroscale parameters, as the assumptions of such a model may possibly either neglected or overemphasised the contribution of one material over the other at leading order.

Even more interesting are the observed discrepancies in both effective Young's Modulus and Poisson's Ratio of the composite material arising as a result of considering near-incompressibility of one microscale component (the large α limit) using the general model, versus incorporating the incompressibility assumption (85) throughout the homogenisation process, as is done in Sect. 3. This indicates again that care must be taken when using an asymptotic homogenisation model for optimising a composite material if one of the component materials has a large bulk modulus, a common occurrence in many industrial fields as absolute incompressibility is an assumption often made for nearly incompressible materials.

Our work shows the importance of fully quantifying the micromechanical properties to ensure that the correct underlying assumptions for the asymptotic homogenisation process are consistent with the measured and/or anticipated microscale parameter ranges. The balance between over simplification and complexity when taking into account micromechanics and geometry of a composite material is a problem for constitutive setups, particularly those more complex than linear elasticity. Restricting this work to purely linear elastic materials, however, has allowed a clearer discussion here of the effects of different limiting behaviours within linear elasticity, such as incompressibility and the effects of comparative shear moduli. By considering slender fibre-supported geometries we are able to reduce the number of dimensions in the microscale allowing us to consider easily generalisable models analytically in detail. This geometry also replicates the physical situation of fibre-reinforced biological tissues such as peripheral nerves, tendons and plant cell walls, as well as those potentially used for fibre-reinforced polymer composites for use in aerospace or construction industries.



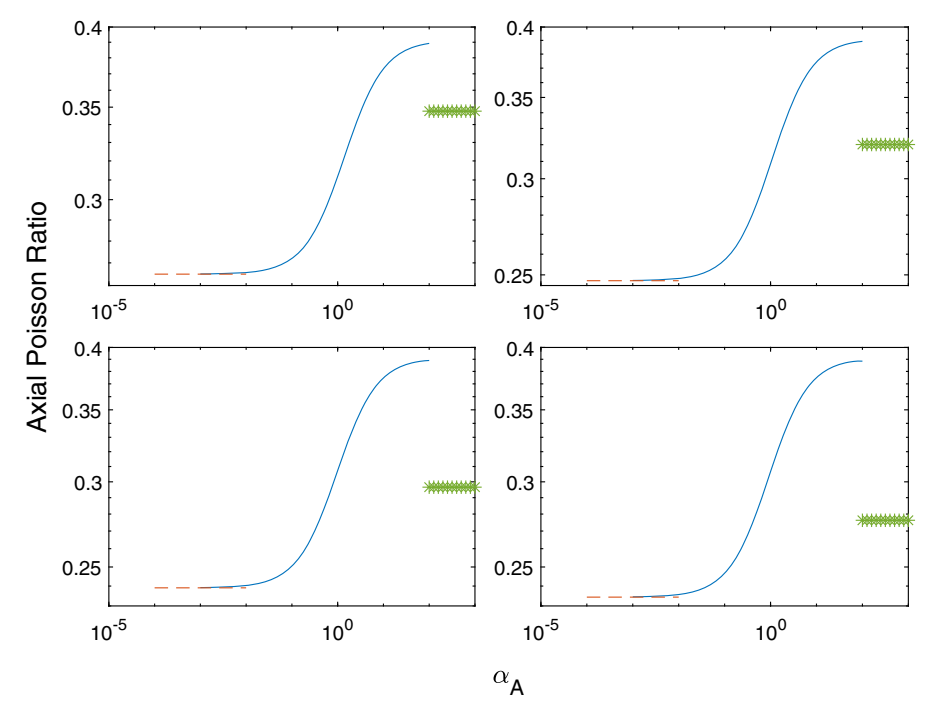


Fig. 8 Plots using simulations of SAH model described in Sect. 2, small μ and large μ , described in Sect. 4.1, for a range of micromechancial properties to show that the small and large limits of the axial Poisson ratio do not match those of the SAH model. Dashed red line denotes small μ simulation and green stars denote large μ simulation. Micromechanical properties are set to $\mu_B = 50$ MPa, $\lambda_B = 0.1$ GPa and $\lambda_A = \alpha_A \mu_A$ where $\mu_A = 50$ MPa (top left), 0.1 GPa (top right), 0.15 GPa (bottom left) or 0.2 GPa (bottom right). (Color figure online)

Many practical applications of fibre-reinforced materials require other, more complex, constitutive setups. A natural next step would be to consider composite materials constructed of non-linear elastic micromechanical materials. However, this would significantly increase the complexity of the microscale setup via additional micromechanical parameters, the relative non-dimensional scalings of which must be carefully considered across various limits. Further theoretical work into fully microscale non-linear behaviour in these limiting cases is thus necessary, as similar discrepancies could arise between asymptotic homogenised models that are based on different scaling assumptions.

Ultimately more experimental work is required to determine the true effective mechanical properties of composite materials. The answer as to whether to use the SAH model in Sect. 2, currently published models such as [26,27], or a limiting microscale behaviour case (*i.e.* the models in Sects. 3 and 4.1) relies on the complex interplay of the orders of α_A , α_B and μ which this paper highlights. Further interdisciplinary work in the limit of incompressibility and extreme shear moduli ratios to fully understand the exact progression of effective properties, such as axial Possion ratio and Young's Moduli, are required in the future.

Acknowledgements The authors would like to thank Professor James Phillips for his advice on biological structures and their mechanical behaviour. EAD would like to thank Professor William Parnell for his advice concerning symmetries and implementing the code. RJS gratefully acknowledges funding from the ESPRC (EP/R004463/1).

Declarations

Conflict of interest The authors declare that they have no conflict of interest.

Open Access This article is licensed under a Creative Commons Attribution 4.0 International License, which permits use, sharing, adaptation, distribution and reproduction in any medium or format, as long as you give appropriate credit to the original author(s)



6 Page 20 of 24 E. A. Doman et al.

and the source, provide a link to the Creative Commons licence, and indicate if changes were made. The images or other third party material in this article are included in the article's Creative Commons licence, unless indicated otherwise in a credit line to the material. If material is not included in the article's Creative Commons licence and your intended use is not permitted by statutory regulation or exceeds the permitted use, you will need to obtain permission directly from the copyright holder. To view a copy of this licence, visit http://creativecommons.org/licenses/by/4.0/.

Appendix A: Effective macroscale stresses for general case

$$\tau_{xx}^{\text{eff}} = (G_{11} + A_1 + A_2 + 2K_{1111}) \frac{\partial u^{(0)}}{\partial x} + (G_{12} + 2K_{1211}) \frac{\partial u^{(0)}}{\partial y} + (G_{21} + 2K_{2111}) \frac{\partial v^{(0)}}{\partial x} + (A_1 - A_2 + G_{22} + 2K_{2211}) \frac{\partial v^{(0)}}{\partial y} + (A_1 - A_2 + G^0 + 2K_{11}^0) \frac{\partial w^{(0)}}{\partial z},$$
(86)

$$\tau_{xy}^{\text{eff}} = (K_{1112} + K_{1121}) \frac{\partial u^{(0)}}{\partial x} + (K_{1212} + K_{1221} + A_2) \frac{\partial u^{(0)}}{\partial y} + (K_{2112} + K_{2121} + A_2) \frac{\partial v^{(0)}}{\partial x} + (K_{2212} + K_{2221}) \frac{\partial v^{(0)}}{\partial y} + (K_{12}^0 + K_{21}^0) \frac{\partial w^{(0)}}{\partial z},$$
(87)

$$\tau_{yy}^{\text{eff}} = (G_{11} + A_1 - A_2 + 2K_{1122})\frac{\partial u^{(0)}}{\partial x} + (G_{12} + 2K_{1222})\frac{\partial u^{(0)}}{\partial y} + (G_{21} + 2K_{2122})\frac{\partial v^{(0)}}{\partial x}$$

$$+(G_{22}+A_1+A_2+2K_{2222})\frac{\partial v^{(0)}}{\partial y}+(G^0+A_1-A_2+2K_{22}^0)\frac{\partial w^{(0)}}{\partial z},$$
(88)

$$\tau_{xz}^{\text{eff}} = (H_{11} + A_2) \left(\frac{\partial u^{(0)}}{\partial z} + \frac{\partial w^{(0)}}{\partial x} \right) + H_{21} \left(\frac{\partial v^{(0)}}{\partial z} + \frac{\partial w^{(0)}}{\partial y} \right), \tag{89}$$

$$\tau_{yz}^{\text{eff}} = H_{12} \left(\frac{\partial w^{(0)}}{\partial x} + \frac{\partial u^{(0)}}{\partial z} \right) + (H_{22} + A_2) \left(\frac{\partial w^{(0)}}{\partial y} + \frac{\partial v^{(0)}}{\partial z} \right)$$
(90)

and

$$\tau_{zz}^{\text{eff}} = (G_{11} + A_1 - A_2) \frac{\partial u^{(0)}}{\partial x} + G_{21} \frac{\partial v^{(0)}}{\partial x} + G_{12} \frac{\partial u^{(0)}}{\partial y} + (G_{22} + A_1 - A_2) \frac{\partial v^{(0)}}{\partial y} + (G_{22} + A_1 - A_2) \frac{\partial v^{(0)}}{\partial y} + (G_{22} + A_1 - A_2) \frac{\partial v^{(0)}}{\partial y}$$

$$+ (G_{22} + A_1 + A_2) \frac{\partial v^{(0)}}{\partial z}.$$
(91)



Appendix B: Effective macroscale elastic tensors for general case

$$C_{11} = 2K_{1111} + G_{11} + A_1 + A_2, (92)$$

$$C_{22} = 2K_{2222} + G_{22} + A_1 + A_2, (93)$$

$$C_{33} = G^0 + A_1 + A_2, (94)$$

$$C_{44} = H_{22} + A_2, (95)$$

$$C_{55} = H_{11} + A_2, (96)$$

$$C_{66} = K_{1221} + K_{1212} + A_2 = K_{2112} + K_{K2121} + A_2, (97)$$

$$C_{12} = 2K_{2211} + G_{22} + A_1 - A_2 = 2K_{1122} + G_{11} + A_1 - A_2, (98)$$

$$C_{13} = G_{11} + A_1 - A_2 = 2K_{11}^0 + G^0 + A_1 - A_2, (99)$$

$$C_{16} = 2K_{2111} + G_{21} = K_{K1211} + \frac{1}{2}G_{12} + \frac{1}{2}K_{1121} + \frac{1}{2}K_{1112} = K_{1112} + K_{1121}, \tag{100}$$

$$C_{23} = G_{22} + A_1 - A_2 = 2K_{22}^0 + G^0 + A_1 - A_2, (101)$$

$$C_{26} = 2K_{1222} + G_{12} = K_{2122} + \frac{1}{2}G_{21} + \frac{1}{2}K_{2212} + \frac{1}{2}K_{2221} = K_{2221} + K_{2212}, \tag{102}$$

$$C_{36} = K_{12}^0 + K_{21}^0 = G_{21} = G_{12} (103)$$

and

$$C_{45} = H_{12} = H_{21}. (104)$$

Appendix C: Cell problem: large μ limit

System A1

$$(1 + \alpha_A) \frac{\partial^2 W_{Ai}^{pq}}{\partial X_k \partial X_i} + \frac{\partial^2 W_{Ak}^{pq}}{\partial X_i \partial X_i} = 0 \quad \text{on } \Omega_A,$$
(105)

with boundary condition on Γ that

$$n_{j}\bar{\mu}\alpha_{A}\left(\frac{\partial W_{Ak}^{pq}}{\partial X_{k}} + \delta_{pq}\right) + \bar{\mu}n_{i}\left(\frac{\partial W_{Ai}^{pq}}{\partial X_{j}} + \frac{\partial W_{Aj}^{pq}}{\partial X_{i}} + \delta_{ip}\delta_{jq} + \delta_{iq}\delta_{jp}\right) = 0.$$

$$(106)$$

System A2

$$(1 + \alpha_A) \frac{\partial^2 W_{Ai}^0}{\partial X_k \partial X_i} + \frac{\partial^2 W_{Ak}^0}{\partial X_i \partial X_i} = 0 \quad \text{on } \Omega_A,$$

$$(107)$$

with boundary condition on Γ that

$$n_{j}\bar{\mu}\alpha_{A}\left(\frac{\partial W_{Ak}^{0}}{\partial X_{k}}+1\right)+\bar{\mu}n_{i}\left(\frac{\partial W_{Ai}^{0}}{\partial X_{j}}+\frac{\partial W_{Aj}^{0}}{\partial X_{i}}\right)=0. \tag{108}$$

System A3

$$\frac{\partial^2 \phi_A^j}{\partial X_i \partial X_i} = 0 \quad \text{on } \Omega_A,$$

with boundary condition on Γ that

$$n_i \bar{\mu} \frac{\partial \phi_A^p}{\partial X_i} + n_p \bar{\mu} = 0.$$



6 Page 22 of 24 E. A. Doman et al.

System B1

$$(1 + \alpha_B) \frac{\partial^2 P_{ji}}{\partial X_k \partial X_i} + \frac{\partial^2 P_{jk}}{\partial X_i \partial X_i} = 0 \quad \text{on } \Omega_B,$$
(109)

with boundary conditions on Γ that

$$P_{ij} = \delta_{ij} \tag{110}$$

and

$$\alpha_B n_j \frac{\partial P_{rk}}{\partial X_k} + n_i \left(\frac{\partial P_{ri}}{\partial X_j} + \frac{\partial P_{rj}}{\partial X_i} \right) = 0. \tag{111}$$

System B2

$$\frac{\partial^2 Q}{\partial X_i \partial X_i} = 0 \quad \text{on } \Omega_B, \tag{112}$$

with boundary conditions on Γ that

$$Q = 1 \tag{113}$$

and

$$n_i \frac{\partial Q}{\partial X_i} = 0. ag{114}$$

Appendix D: Cell problem: small α case

System 1:

$$\frac{\partial^2 W_{Ai}^{pq}}{\partial X_k \partial X_i} + \frac{\partial^2 W_{Ak}^{pq}}{\partial X_i \partial X_i} = 0 \quad \text{on } \Omega_A, \tag{115}$$

and

$$(1 + \alpha_B) \frac{\partial^2 W_{Bi}^{pq}}{\partial X_i \partial X_i} + \frac{\partial^2 W_{Bi}^{pq}}{\partial X_k \partial X_i} + \frac{\partial^2 W_{Bk}^{pq}}{\partial X_i \partial X_i} = 0 \quad \text{on } \Omega_B,$$
(116)

with boundary conditions on Γ that

$$W_{Ak}^{pq} = W_{Bk}^{pq} \tag{117}$$

and

$$\mu n_{i} \left(\frac{\partial W_{Ai}^{pq}}{\partial X_{j}} + \frac{\partial W_{Aj}^{pq}}{\partial X_{i}} \right) + n_{i} (\mu - 1) (\delta_{ip} \delta_{jq} + \delta_{iq} \delta_{jp}) = n_{j} \alpha_{B} \left(\frac{\partial W_{Bk}^{pq}}{\partial X_{k}} + \delta_{pq} \right)$$

$$+ n_{i} \left(\frac{\partial W_{Bi}^{pq}}{\partial X_{i}} + \frac{\partial W_{Bj}^{pq}}{\partial X_{i}} \right).$$

$$(118)$$

System 2:

$$\frac{\partial^2 W_{Ai}^0}{\partial X_k \partial X_i} + \frac{\partial^2 W_{Ak}^0}{\partial X_i \partial X_i} = 0 \quad \text{on } \Omega_A, \tag{119}$$

and

$$(1 + \alpha_B) \frac{\partial^2 W_{Bi}^0}{\partial X_k \partial X_i} + \frac{\partial^2 W_{Bk}^0}{\partial X_i \partial X_i} = 0 \quad \text{on } \Omega_B,$$
(120)



with boundary conditions on Γ that

$$W_{Ak}^0 = W_{Bk}^0 (121)$$

and

$$\mu n_i \left(\frac{\partial W_{Ai}^0}{\partial X_j} + \frac{\partial W_{Aj}^0}{\partial X_i} \right) = n_j \alpha_B \left(\frac{\partial W_{Bk}^0}{\partial X_k} + 1 \right) + n_i \left(\frac{\partial W_{Bi}^0}{\partial X_j} + \frac{\partial W_{Bj}^0}{\partial X_i} \right). \tag{122}$$

System 3:

$$\frac{\partial^2 \phi_A^p}{\partial X_i \partial X_i} = 0 \quad \text{on } \Omega_A, \tag{123}$$

with a counterpart equation for B and boundary equations on Γ that

$$\phi_A^P = \phi_B^P \tag{124}$$

and

$$n_i \left(\mu \frac{\partial \phi_A^p}{\partial X_i} - \frac{\partial \phi_B^p}{\partial X_i} \right) + n_p(\mu - 1) = 0.$$
 (125)

References

- 1. Mangalgiri P (1999) Composite materials for aerospace applications. Bull Mater Sci 22(3):657-664
- 2. Saba N, Jawaid M, Sultan MT (2018) An overview of mechanical and physical testing of composite materials. Elsevier, Amsterdam
- 3. Sheffield C, Meyers K, Johnson E, Rajachar RM (2018) Application of composite hydrogels to control physical properties in tissue engineering and regenerative medicine. Gels 4(2):51
- 4. Greenhall J, Homel L, Raeymaekers B (2019) Ultrasound directed self-assembly processing of nanocomposite materials with ultra-high carbon nanotube weight fraction. J Compos Mater 53(10):1329–1336
- 5. Lakes R (1993) Materials with structural hierarchy. Nature 361(6412):511–515
- Khalesi H, Lu W, Nishinari K, Fang Y (2021) Fundamentals of composites containing fibrous materials and hydrogels: a review on design and development for food applications. Food Chem 364:130329
- Mertiny P, Ellyin F (2002) Influence of the filament winding tension on physical and mechanical properties of reinforced composites. Composites Part A 33(12):1615–1622
- 8. Ebenstein DM, Pruitt LA (2006) Nanoindentation of biological materials. Nano Today 1(3):26-33
- 9. Hemker K, Sharpe W (2007) Microscale characterization of mechanical properties. Annu Rev Mater Res 37(1):93-126
- Dixit A, Mali HS (2013) Modeling techniques for predicting the mechanical properties of woven-fabric textile composites: a review. Mech Compos Mater 49(1):1–20
- 11. Fang F, Lake SP (2016) Modelling approaches for evaluating multiscale tendon mechanics. Interface Focus 6(1):20150044
- 12. Haghighi M, Golestanian H, Aghadavoudi F (2021) Determination of mechanical properties of two-phase and hybrid nanocomposites: experimental determination and multiscale modeling. J Polym Eng 41(5):356–364
- 13. Khezrzadeh H (2017) A statistical micromechanical multiscale method for determination of the mechanical properties of composites with periodic microstructure. Composites Part B 115:138–143
- Lurie SA, Belov PA, Tuchkova NP (2005) The application of the multiscale models for description of the dispersed composites.
 Composites Part A 36(2):145–152
- 15. Piatnitski A, Ptashnyk M (2017) Homogenization of biomechanical models for plant tissues. Multiscale Model Simul 15(1):339–387
- Buljac A, Shakoor M, Neggers J, Bernacki M, Bouchard PO, Helfen L, Morgeneyer TF, Hild F (2017) Numerical validation framework for micromechanical simulations based on synchrotron 3d imaging. Comput Mech 59(3):419–441
- 17. Lebensohn RA, Brenner R, Castelnau O, Rollett AD (2008) Orientation image-based micromechanical modelling of subgrain texture evolution in polycrystalline copper. Acta Mater 56(15):3914–3926
- Masad E, Tashman L, Somedavan N, Little D (2002) Micromechanics-based analysis of stiffness anisotropy in asphalt mixtures. J Mater Civil Eng 14(5):374–383
- 19. Hill R (1963) Elastic properties of reinforced solids: some theoretical principles. J Mech Phys Solids 11(5):357–372
- 20. Hill R (1964) Theory of mechanical properties of fibre-strengthened materials. 1: elastic behaviour. J Mech Phys Solids 12(4):199–212
- 21. Hashin Z (1979) Analysis of properties of fiber composites with anisotropic constituents. J Appl Mech Trans ASME 46(3):543–550
- Hori M, Nemat-Nasser S (1999) On two micromechanics theories for determining micro-macro relations in heterogeneous solids.
 Mech Mater 31(10):667–682



6 Page 24 of 24 E. A. Doman et al.

- 23. Lanir Y (1983) Constitutive equations for fibrous connective tissues. J Biomech 16(1):1–12
- 24. Mori T, Tanaka K (1973) Average stress in matrix and average elastic energy of materials with misfitting inclusions. Acta Metall 21(5):571–574
- Pinho-da Cruz J, Oliveira J, Teixeira-Dias F (2009) Asymptotic homogenisation in linear elasticity. Part I: mathematical formulation and finite element modelling. Comput Mater Sci 45(4):1073–1080
- Parnell WJ, Abrahams ID (2008) Homogenization for wave propagation in periodic fibre-reinforced media with complex microstructure. I-Theory. J Mech Phys Solids 56(7):2521–2540
- Penta R, Gerisch A (2015) Investigation of the potential of asymptotic homogenization for elastic composites via a three-dimensional computational study. Comput Vis Sci 17(4):185–201
- 28. Penta R, Gerisch A (2017) The asymptotic homogenization elasticity tensor properties for composites with material discontinuities. Continuum Mech Thermodyn 29(1):187–206
- Ramírez-Torres A, Penta R, Rodríguez-Ramos R, Merodio J, Sabina FJ, Bravo-Castillero J, Guinovart-Díaz R, Preziosi L, Grillo A (2018) Three scales asymptotic homogenization and its application to layered hierarchical hard tissues. Int J Solids Struct 130–131:190–198
- Davit Y, Bell CG, Byrne HM, Chapman LA, Kimpton LS, Lang GE, Leonard KH, Oliver JM, Pearson NC, Shipley RJ, Waters SL, Whiteley JP, Wood BD, Quintard M (2013) Homogenization via formal multiscale asymptotics and volume averaging: how do the two techniques compare? Adv Water Resour 62:178–206
- 31. Burridge R, Keller JB (1981) Poroelasticity equations derived from microstructure. J Acoust Soc Am 70(4):1140
- 32. Chen MJ, Kimpton LS, Whiteley JP, Castilho M, Malda J, Please CP, Waters SL, Byrne HM (2020) Multiscale modelling and homogensation of fibre-reinforced hydrogels for tissue engineering. Eur J Appl Math 31(1):143–171
- Daly KR, Roose T (2018) Determination of macro-scale soil properties from pore-scale structures: model derivation. Proc R Soc A 474(2209):20170141
- Meguid SA, Kalamkarov AL (1994) Asymptotic homogenization of elastic composite materials with a regular structure. Int J Solids Struct 31(3):303–316
- 35. Bauchau O, Craig J (2009) Structural analysis. Springer, Dordrecht
- 36. Parnell WJ, Vu MB, Grimal Q, Naili S (2012) Analytical methods to determine the effective mesoscopic and macroscopic elastic properties of cortical bone. Biomech Model Mechanobiol 11(6):883–901
- 37. Nolan D, McGarry J (2016) On the compressibility of arterial tissue. Ann Biomed Eng 44(4):993–1007
- 38. Saraf H, Ramesh K, Lennon A, Merkle A, Roberts J (2007) Mechanical properties of soft human tissues under dynamic loading. J Biomech 40(9):1960–1967
- 39. Howell P, Kozyreff G, Ockendon J (2009) Applied solid mechanics, vol 4343. Cambridge University Press, Cambridge

Publisher's Note Springer Nature remains neutral with regard to jurisdictional claims in published maps and institutional affiliations.

